GIScience & Remote Sensing

ISSN: 1548-1603 (Print) 1943-7226 (Online) Journal homepage: www.tandfonline.com/journals/tgrs20

Earlier snowmelt is driving the northward migration of East Asian Sand and Dust Storms

Lilin Zheng, Xia Lin , Annah Lake Zhu , Ruishan Chen & Ling Wang

To cite this article: Lilin Zheng, Xia Lin , Annah Lake Zhu , Ruishan Chen & Ling Wang (2026) Earlier snowmelt is driving the northward migration of East Asian Sand and Dust Storms, GIScience & Remote Sensing, 63:1, 2604385, DOI: 10.1080/15481603.2025.2604385

To link to this article: https://doi.org/10.1080/15481603.2025.2604385

GISCIENCE & REMOTE SENSING
2026, VOL. 63, NO. 1, 2604385
https://doi.org/10.1080/15481603.2025.2604385

Taylor & Francis
Taylor & Francis Group

RESEARCH ARTICLE

OPEN ACCESS Check for updates

Earlier snowmelt is driving the northward migration of East Asian Sand and Dust Storms

Lilin Zheng[a,b], Xia Lin[a], Annah Lake Zhu[c], Ruishan Chen[a,b] and Ling Wang[a]

[a]Department of Landscape Architecture, School of Design, Shanghai Jiao Tong University, Shanghai, People's Republic of China; [b]Digital Engineering Technology Innovation Center for Territorial Ecological Governance, Ministry of Natural Resources, Shanghai, People's Republic of China; [c]Environmental Policy Group, Wageningen University, Wageningen, Netherlands

ABSTRACT

Recent decades have witnessed significant shifts in sand and dust storm patterns across East Asia, yet the exact spatiotemporal patterns and mechanisms driving these changes remain unclear. Here, we analyzed daily meteorological observations and satellite aerosol products to derive dust optical depth, sand and dust storm (SDS) frequency, and related indices for 2001–2024. Our results show that SDS is concentrated in northern China and southern Mongolia and exhibits a clear northward migration. Partial-correlation analyses reveal that, in sparsely vegetated regions, pre-season snow cover exerts a stronger negative control on spring dust activity than vegetation cover. Both generalized linear models and structural equation modeling further reveal that, in these low-vegetated regions, soil moisture generated from late winter snow cover is the primary factor mitigating dust generation, with wind speed remaining a contributing, but vegetation-independent, factor. By contrast, in highly vegetated regions, vegetation is the dominant dust suppression mechanism, primarily through attenuating wind speed. Our results suggest that the observed northward shift in SDS is driven primarily by reduced winter snow cover and earlier snowmelt under warming, rather than by insufficient afforestation, thus underscoring the pivotal role of cryospheric changes in modulating aeolian processes.

ARTICLE HISTORY
Received 6 October 2025
Accepted 10 December 2025

KEYWORDS
Sand and Dust Storms; snow cover; vegetation dynamics; climate warming; East Asia

1. Introduction

Desert dust plays a significant role in aerosol radiative forcing, biogeochemical cycling, and agricultural productivity (Filonchyk 2022; Li et al. 2022), and is also a major natural hazard affecting human health, transportation, infrastructure, and a range of economic activities (Middleton 1991; Park and Choi 2016). East Asia's desert dust source regions are among the largest global emitters, releasing approximately 500–1100 Tg of dust into the atmosphere annually (Zhang, Arimoto, and An 1997; Kim et al. 2024). Within mobile and stabilised dune interiors, limited precipitation and low vegetation make the aeolian processes of sediment erosion, transport, and deposition largely uncontrollable (Gao, Narteau, and Gadal 2021; Naeimi et al. 2023). In contrast, at desert margins, aeolian dynamics are shaped by a combination of human activity, precipitation (including snowfall), and surface cover, with severe dust events frequently impacting densely populated regions (D'Odorico et al. 2007).

Numerous studies have highlighted the positive role of vegetation in mitigating sand and dust storms (SDS) at desert margins (Wang et al. 2021; Wang et al. 2022), which has been a key motivator behind China's large-scale afforestation projects. Notable examples include the Three-North Shelterbelt Project along the edges of the Tengger Desert, the Mu Us Desert, and the recently completed "edge-locking" project in the Taklamakan Desert (Cheng et al. 2025; Yan et al. 2025). These efforts aim to reduce the impact of SDS on oasis regions through tree planting and other engineering measures. However, despite these initiatives, the frequency and scope of dust events indicate that "edge-locking" projects have not effectively curtailed SDS

CONTACT Ruishan Chen rschen@sjtu.edu.cn
Supplemental data for this article can be accessed online at https://doi.org/10.1080/15481603.2025.2604385.

occurrences. In 2023, China recorded 17 dust events, five of which reached storm intensity, setting a decade-high record (Wu et al. 2025). This raises a critical question: Can vegetation truly prevent SDS? What other factors beyond vegetation contribute to the formation of SDS? These questions remain inadequately addressed.

While some studies suggest that recent desert dust sources affecting China are primarily from Mongolia (Chen et al. 2023), it is important to note that the Gobi Desert in Mongolia has been recognised as a major dust source for many decades (Middleton 1991; Natsagdorj, Jugder, and Chung 2003). What recent analyses indicate, however, is that Mongolia's relative contribution to SDS impacting northern China has increased in recent years (Chen et al. 2023; Wu et al. 2025). Government officials and researchers often attribute this to insufficient afforestation efforts in Mongolia, which have exacerbated land desertification (Lee and Sohn 2011; Bao et al. 2023). However, satellite observations reveal a predominant greening trend across vast northern regions, including Mongolia, with this trend being particularly pronounced in early spring due to earlier phenological shifts (Piao et al. 2015; Lian et al. 2022; Jiang, Shen, and Yang 2025). Another significant, yet often overlooked, change alongside vegetation is the reduction in winter snow cover (Yang, Peng, and Dan 2025). Snow cover decline exposes more soil, especially toward the end of the cold season, as accelerated snowmelt leaves previously snow-covered land unprotected, making it more vulnerable to wind erosion and SDS formation (Yin et al. 2022). As temperatures rise in spring, the soil becomes drier and looser, further enhancing its susceptibility to wind erosion and contributing to the intensity of SDS (Meinander et al. 2022; Hall et al. 2021b). Collectively, these findings indicate that the increasing influence of Mongolian sources on SDS over northern China cannot be satisfactorily explained by afforestation deficits alone, but instead calls for attribution frameworks that jointly account for snow and vegetation, soil hydrothermal conditions and atmospheric circulation.

Several recent studies have explored how snow cover and snowmelt influence SDS activity in the Gobi and other cold or arid regions (Amino et al. 2021; Maki et al. 2022; Meinander et al. 2025), this snow–SDS linkage has still received less attention than vegetation effects. In particular, it remains unclear, at the scale of the East Asian desert margins, whether snow or vegetation exerts the dominant control on current SDS activity. Here we hypothesise that, in regions with low vegetation cover, snow dynamics play a more dominant role in regulating wind and sand activity in the subsequent year than relatively small interannual changes in vegetation cover. Under this hypothesis, climate warming, by reducing winter–spring snow cover across northern regions and shortening the duration of snow protection, is gradually transforming these areas into increasingly important sources of SDS.

To evaluate this hypothesis, satellite and ground-based observations were integrated within a unified statistical framework. East Asian dust events were identified using daily dust aerosol concentrations from MODIS Deep Blue Collection 6.1, together with observational records of floating dust, blowing sand and sand storms from 632 meteorological stations, so that both the intensity and displacement of SDS could be characterised. Additionally, partial correlation analysis, generalised linear models, and structural equation modelling (SEM) were used to simulate and compare the effects and driving mechanisms of both vegetation and snow cover on dust activity across different levels of vegetation cover. The results offer new insights into the mechanisms driving changes in dust activity in East Asia in order to inform China's desertification management strategies.

2. Materials and methods

2.1. Study region

This study focuses on dust activity in the Three-North Shelterbelt Project area (China) and Mongolia (Figure 1). Given that SDS in the mobile and stabilised dunes is primarily driven by wind, with minimal influence from vegetation and snow, this study focuses on the "desert edge area"—regions where dust activity, vegetation, and snow cover overlap. Specifically, the study area is defined as regions where the annual frequency of dust aerosol optical depth (*DOD*), snow cover frequency (*SCF*), and Normalised Difference Vegetation Index (*NDVI*) > 0 simultaneously exceeds 30% between 2001 and 2024. These areas, located at the desert periphery, serve as a basis for analysing the interactions between vegetation,

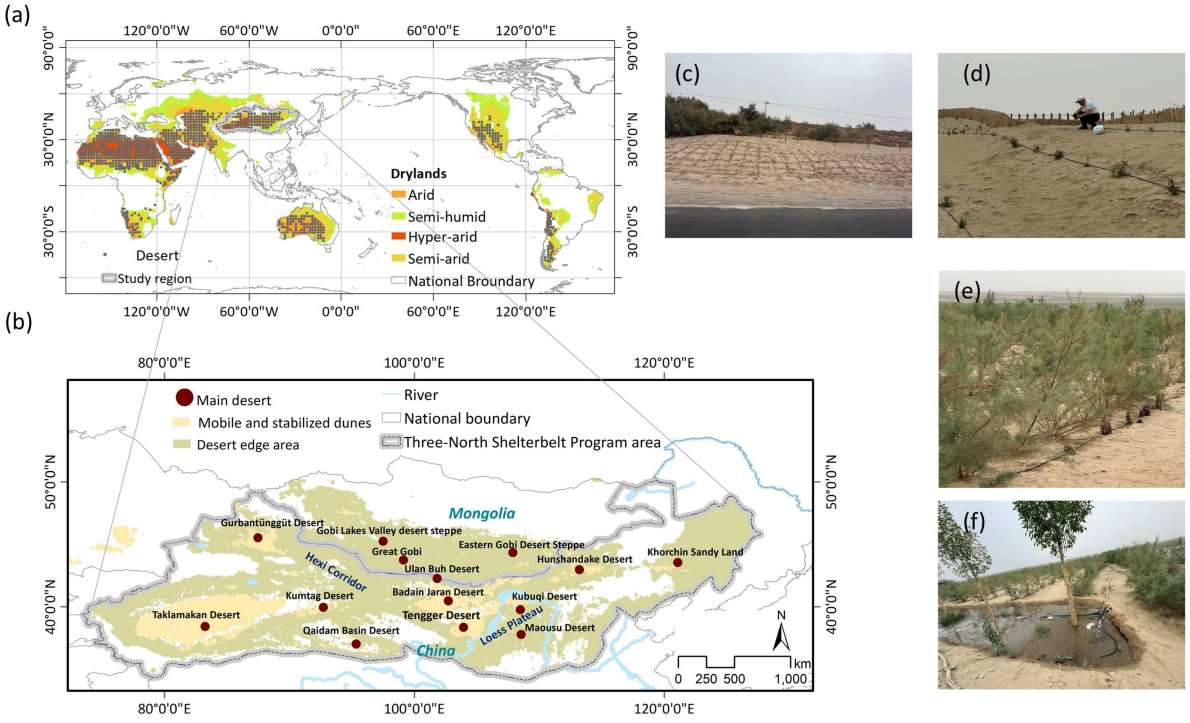

Figure 1. Location of the study region (a and b). The distribution of mobile and stabilised dunes is based on Zheng et al. (2024). Panels (c)-(f) display photos of the Chinese government's "edge-locking" projects along the desert margins of the Taklamakan and other deserts. These efforts have involved substantial financial and human resources in planting species such as *Tamarix* (salt cedar) and *Alhagi* (camelthorn) to combat desertification.

snow, and dust. In contrast, regions where *DOD* is frequently greater than 0 but *NDVI* and *SCF* are very low correspond to the core desert (roughly equivalent to mobile and stabilised dunes) and are therefore excluded from this study.

In addition, SDS activity in East Asia is largely concentrated in spring, reflecting the combined influence of the Mongolian high-pressure system and regional vegetation phenology (Figure S1). Accordingly, this study focuses on the spring months, March–May.

2.2. Dust activity analysis using ground-based observations and remote sensing data

(1) Ground-based dust observations

The meteorological record of SDS from 2001 to 2024 was obtained from the China Meteorological Administration (2025). This dataset includes continuous daily dust activity observations from 632 stations across northern China over the 24-year period. Dust events were classified according to the China National Standard GB/T 20480-2017. Floating dust (horizontal visibility < 10 km; near-surface wind speed < 3 m/s), blowing sand (1 < horizontal visibility ≤ 10 km), and sand storms (horizontal visibility ≤ 1 km) are defined and used in this study. Additionally, the comprehensive dust index (*CDI*) for each station was calculated as follows:

$$CDI = \text{floating dust} \times 1 + \text{blowing sand} \times 2 + \text{sand storm} \times 3 \quad (1)$$

(2) Remote sensing data and *DOD* calculation

Dust Aerosol Optical Depth (*DOD*) for the period 2001–2024 across the study region was retrieved using MODIS DB Collection 6.1 aerosol products from the Aqua (MYD04_L2) and Terra (MOD04_L2) platforms. These Level-2 products have a native footprint of approximately 10 km and employ the Deep Blue

algorithm to detect terrestrial aerosol loads over bright land surfaces based on blue-band radiances (Anderson et al. 2005).

The aerosol products consist of Aerosol Optical Depth (*AOD*) at 550 nm, single scattering albedo (*SSA*) at 470 nm, and the Ångström exponent (*AE*). Prior to calculating *DOD* values, *AOD*, *SSA*, and*AE* were mapped from the native swath to a regular $0.1^\circ \times 0.1^\circ$ grid (comparable in scale to the native footprint) using a nearest-neighbour cell-assignment scheme. This preserves the original retrievals without introducing additional spatial smoothing and is widely used in previous studies deriving *DOD* from MODIS Deep Blue products (Kok et al. 2017; Pu and Ginoux 2018; Yao et al. 2024). Sensitivity tests with bilinear and inverse-distance-weighted interpolation yielded *DOD* fields and trends that were nearly indistinguishable from those based on the nearest-neighbour scheme, and therefore the nearest-neighbour interpolation was adopted in all subsequent analyses. To minimise the influence of low-quality data, only *AOD* measurements classified as high or very high quality were used for the *DOD* retrieval (Kok et al. 2017).

DOD was calculated using the method outlined by Pu and Ginoux (2018), which separates the contributions of fine particles and coarse-mode dust from the AOD:

$$DOD = AOD \times 0.98 - 0.5098\alpha + 0.0512\alpha^2 \tag{2}$$

$$(\omega < 0.99) \tag{3}$$

Here, α is the AE at 470 nm and ω is the SSA. Dust absorption of solar radiation and its separation from other scattering aerosols, such as sea salt, are considered when $\omega < 0.99$.

Daily *DOD* values were calculated by averaging the Terra and Aqua *DOD* when both were available, or by using data from the available platform when only one set was accessible (Pu and Ginoux 2018; Wang et al. 2021). The monthly mean *DOD*, and sand and dust storm frequency (*DSF*, number of days when *DOD* > 0.2) (Ginoux et al. 2012) were then calculated for northern China and Mongolia.

2.3. Vegetation cover and snow metrics

(1) Snow cover frequency (*SCF*) and start of melting date (*SOM*)

Snow indices and phenological metrics were derived from the MODIS/Terra Snow Cover Daily Global 500 m product (MOD10A1, Collection 6.1; Hall et al. 2002, Hall, Salomonson, and Riggs 2021a). In this product, the NDSI_Snow_Cover band stores the fractional snow-covered area within each 500 m pixel as an integer between 0 and 100 (%), whereas values outside this range (e.g. 200, 201, 211, 237, 239, 250, 254, 255) are quality or condition flags indicating cloud, night, water, or missing data (Hall et al. 2002; Hall, Salomonson, and Riggs 2021a). In this study, only pixels with NDSI_Snow_Cover values in the 0–100 range were retained as valid snow retrievals, and all flag values were masked as missing. NDSI_Snow_Cover was then normalised from its original 0–100% range to a 0–1 range by division by 100; this normalised quantity is hereafter referred to as fractional snow cover (*f_snow*).

To reduce the impact of clouds and atmospheric interference, an 8-day maximum-value compositing to the daily *f_snow* time series was applied and then smoothed the composites using the Savitzky–Golay filter (Savitzky and Golay 1964). Monthly snow cover frequency (*SCF*) for each pixel and year was calculated as the fraction of days within a given month with *f_snow* ≥ 0.1, following previous work that uses 0.1 as a conservative threshold separating snow-covered and snow-free conditions (He et al. 2024, Zhang et al. 2019a).

The start of melt date (*SOM*) was then defined as the first day in a given year when the smoothed*f_snow* remained below 0.1 for at least five consecutive days, indicating the persistent disappearance of the seasonal snowpack.

(2) Vegetation index and fractional vegetation coverage (FVC)

The Normalised Difference Vegetation Index (*NDVI*) was used as the primary vegetation index due to its strong correlation with canopy density and aboveground biomass (Tucker 1979, Smith et al. 2019). *NDVI* is calculated as:

$$NDVI = \frac{\rho_{NIR} - \rho_{Red}}{\rho_{NIR} + \rho_{Red}} \tag{4}$$

where ρ_{NIR} and ρ_{Red} were derived from Band 2 (NIR: 841–876 nm) and Band 1 (red: 620–670 nm) of the MODIS surface reflectance eight-day product (MOD09A1 v6), respectively. *NDVI* was used to represent the monthly maximum vegetation cover.

To compare the impacts of vegetation and snow on dust activity across different vegetation coverages, fractional vegetation coverage (FVC) was calculated. FVC is defined as:

$$FVC = \frac{NDVI - \mathrm{NDVI}_{min}}{\mathrm{NDVI}_{max} - \mathrm{NDVI}_{min}} \tag{5}$$

where NDVI_{max} and NDVI_{min} represent the *NDVI* values of fully covered vegetation and bare soil, respectively. To reduce uncertainty in determining extreme *NDVI* values, the *NDVI* values at the 5% and 95% percentiles from the surface grid values were selected as NDVI_{min} and NDVI_{max}, respectively.

2.4. Hydro-climate context

(1) Wind speed, temperature, and precipitation data sources

In this study, daily wind speed, temperature and precipitation were obtained from 632 surface stations maintained by the China Meteorological Administration (2025), and from ERA5 reanalysis (Service Copernicus Climate Change, 2017). These homogenised station records are available only within China, and no long-term dust and meteorological station network in Mongolia is available that is directly comparable to the China Meteorological Administration (CMA) dataset in terms of observing standards and event coding. Accordingly, in the attribution of station-based dust activity (*CDI*), collocated CMA station meteorological observations were used, whereas in the attribution analyses based on satellite-derived *DOD* and *DSF*, ERA5 meteorological fields at the grid scale were used.

(2) Drought indices

The Standardised Precipitation Evapotranspiration Index (SPEI) at the 3- and 6-month scales, calculated based on daily temperature and precipitation data from 2001 to 2024, was used to assess regional drought condition. The SPEI is based on the climatic water balance between precipitation and potential evapotranspiration (PET) and combines the sensitivity of the Palmer Drought Severity Index with the multi-temporal flexibility of the Standardised Precipitation Index (Vicente-Serrano, Beguería, and López-Moreno 2010). For each month i, water balance was calculated as follows:

$$D_i = P_i - PET_i \tag{6}$$

Where P_i is monthly precipitation and PET_i is monthly potential evapotranspiration derived from station-based meteorological data. The water-balance series was then accumulated over different time scales k (k = 3, 6 months in this study):

$$D_i^{(k)} = \sum_{j=0}^{k-1} D_{i-j} \tag{7}$$

Where $D_i^{(k)}$ is the k-month accumulated climatic water balance at month i, obtained by summing the monthly water-balance series D over the current month and the preceding $k - 1$ months. The resulting $D_i^{(k)}$ series was fitted to a log-logistic probability distribution. The cumulative probability was finally transformed into a standardised normal variable with mean zero and unit variance, yielding the SPEI at time scale k. Negative SPEI values indicate drier-than-normal conditions, while positive values indicate wetter-than-normal conditions. In this study, $SPEI_3$ and $SPEI_6$ were used to represent short- and medium-term moisture conditions, respectively.

(3) Evapotranspiration data sources

Evapotranspiration data, including vegetation transpiration (*Ec*), soil evaporation (*Es*) and canopy interception (*Ei*), were obtained from the Penman–Monteith–Leuning evapotranspiration Version 2 (PML_V2) product (Gan et al. 2018; Zhang et al. 2019b). PML_V2 provides global land-surface ET and gross primary production (GPP) at 500 m spatial resolution and 8-day temporal resolution for the period 2000–2023, covering latitudes from 60°S to 90°N. The PML_V2 estimates have been evaluated against

observations from 95 eddy-covariance flux sites worldwide and shown to be reliable (Zhang et al. 2019b). These data were used to quantify the exchange of water vapour among the atmosphere, vegetation and soil in our study region.

(4) Soil moisture data sources

Soil moisture fields were obtained from the NASA Global Land Data Assimilation System Version 2.2 (GLDAS-2.2) Catchment land-surface model daily product at $0.25° \times 0.25°$ spatial resolution (Li et al. 2019). GLDAS-2.2 provides globally consistent land-surface states and fluxes from 2003 to the present, based on the CLSM-F2.5 model with GRACE data assimilation. The surface soil moisture (SoilMoist_S_tavg, 0–2 cm) and profile soil moisture (SoilMoist_P_tavg, integrated soil column) were used to represent near-surface and vertically integrated soil water conditions.

These hydro-climate variables, such as wind speed, drought indices, soil moisture, and evapotranspiration, were used to explore the mechanisms underlying the interactions between vegetation, snow, and dust activity (Table 1).

2.5. Analysis

(1) Trend analysis

The Mann–Kendall (MK) trend test is applied for identifying temporal variation patterns in vegetation and their influencing factors. The null hypothesis assumed no trend at the 0.05 confidence level (p value). A positive change slope (z value) indicates an increasing trend, while a negative z value signifies a decreasing trend (Hamed and Ramachandra Rao 1998).

(2) Partial correlation analysis

Partial correlation analyses were conducted to examine the responses of dust activity to snow cover and vegetation. Spring dust activity was represented by *DOD*, *DSF* and *CDI* for March–May of each year. When assessing the effects of snow cover, partial correlation coefficients were calculated between these spring dust indices and the mean snow-cover frequency (*SCF*) in the preceding 1, 2,…, n months (i.e. winter and early-spring months before March–May), while controlling for the corresponding March–May *NDVI* and maximum wind speed ($Wind_{\max}$). When assessing the effects of vegetation, analogous partial correlations were computed using pre-season *NDVI* as the predictor and controlling for *SCF* and $Wind_{\max}$. Because vegetation activity is largely dormant in mid-winter, lagged winter *NDVI* was not considered. A three-month pre-season window (SCF_{pre3}) was ultimately adopted, as it showed the strongest and most spatially coherent influence on *DOD*, *DSF* and *CDI* across the study region.

(3) Generalised linear model

To quantify how snow, vegetation, humidity and wind jointly influence station-level dust activity, the Zero-Inflated Negative Binomial (ZINB) regression model was applied. ZINB is a member of the generalised linear model family, specifically designed for overdispersed count data with excess zeros (e.g. when no dust event is recorded) (Faroughi and Ismail 2017).

The response variable is the monthly dust activity index (*CDI*) at 632 meteorological stations, derived from daily observations of floating dust, blowing sand, and sand and dust storms. *CDI* was aggregated to monthly values for March, April and May over the period 2001–2024. For each station–month, explanatory variables were constructed at the same temporal resolution. Wind speed and the SPEI were derived from station-based meteorological records. Vegetation and snow-cover indicators were calculated as spatial averages within a 30 km buffer around each station, using the corresponding gridded remote-sensing products. Because dust activity can be influenced by antecedent drought, snow and vegetation conditions, we initially constructed a comprehensive candidate predictor set that included both current-month values and 1–3 month lags of these variables. Before model fitting, missing values were interpolated using a sliding-average method, and all predictors were standardised to have a mean of zero and a standard deviation of one so that the regression coefficients are directly comparable in magnitude and represent standardised effect sizes. To avoid multicollinearity and obtain a parsimonious model, we applied the variance inflation factor (VIF) to the full candidate predictor set. For each predictor x_k, the VIF is defined as:

$$VIF_k = 1 / (1 - R_k^2), \tag{8}$$

Table 1. Summary of variables used in the dust activity, climate, vegetation, snow, soil moisture and evapotranspiration analyses.

Variable category	Variable name	Meaning	Time span	Data source
Dust activity	*DOD*	Dust Aerosol Optical Depth	2001–2024	MOD04_L2 / MYD04_L2
	DSF	Dust storm frequency	2001–2024	MOD04_L2 / MYD04_L2
	CDI	Comprehensive Dust Index	2001–2024	632 CMA stations
Vegetation cover	*NDVI*	Monthly maximum Normalised Difference Vegetation Index	2001–2024	MOD09A1 Collection 6.1
	$NDVI0.\ 1_{ratio}$	Fractional area with NDVI > 0.1 within station buffer	2001–2024	MOD09A1 Collection 6.1
	$NDVI0.\ 3_{ratio}$	Fractional area with NDVI > 0.3 within station buffer	2001–2024	MOD09A1 Collection 6.1
Snow metrics	*SCF*	Snow cover frequency in the current month	2001–2024	MOD10A1.061
	SCF_{pre3}	Pre-season snow cover frequency over the previous 3 months	2001–2024	MOD10A1.061
	SOM	Start of melt date	2001–2024	MOD10A1.061
Wind	$Wind_{avg}$	Monthly mean near-surface wind speed	2001–2024	632 CMA stations and ERA5
	$Wind_{max}$	Monthly maximum near-surface wind speed	2001–2024	632 CMA stations and ERA5
Drought indices	$SPEI_3$	Standardised Precipitation–Evapotranspiration Index at 3-month scale	2001–2024	632 CMA stations and ERA5
	$SPEI_6$	Standardised Precipitation–Evapotranspiration Index at 6-month scale	2001–2024	632 CMA stations and ERA5
Evapotranspiration	*Ec*	Vegetation transpiration component of evapotranspiration	2001–2023	global ET–GPP product
	Es	Soil evaporation component of evapotranspiration	2001–2023	global ET–GPP product
	Ei	Interception loss from vegetation canopy	2001–2023	global ET–GPP product
Soil moisture	*SM_s*	Surface soil moisture	2003–2024	GLDAS v2.2
	SM_p	Profile soil moisture	2003–2024	GLDAS v2.2

Where R_k^2 is the coefficient of determination obtained by regressing x_k on all other predictors. Large VIF values indicate that a predictor can be well explained by a linear combination of the remaining predictors and therefore suffers from multicollinearity. In this study, we iteratively removed predictors with VIF > 5 and recomputed VIFs until all remaining predictors had VIF < 5. The final set of predictors retained after this screening is shown in Equations (9a)-9(b).

The ZINB model was fitted separately for two vegetation-cover regimes (FVC < 0.5 and FVC ≥ 0.5) to distinguish low- and high-vegetation conditions. It consists of two linked components: (i) a count component, which models the expected frequency of dust events (*CDI_count*), and (ii) a zero-inflation component, which models the Bernoulli process determining whether a station–month is in a "susceptible" state for dust (*CDI_prob*). The model can be written as:

$$\log(\mu i) = \beta_0 + \beta_1 \cdot SPEI_3 + \beta_2 \cdot SPEI_6 + \beta_3 \cdot NDVI + \beta_4 \cdot NDVI0.1_{ratio} + \beta_5 \cdot NDVI0.3_{ratio} + \beta_6 \cdot SCF + \beta_7 \cdot SCF_{pre3} + \beta_8 \cdot Wind_{avg} + \beta_9 \cdot Wind_{\max} \quad (9a)$$

$$\text{logit}(\pi i) = \gamma_0 + \gamma_1 \cdot SPEI_3 + \gamma_2 \cdot SPEI_6 + \gamma_3 \cdot NDVI + \gamma_4 \cdot NDVI0.1_{ratio} + \gamma_5 \cdot NDVI0.3_{ratio} + \gamma_6 \cdot SCF + \gamma_7 \cdot SCF_{pre3} + \gamma_8 \cdot Wind_{avg} + \gamma_9 \cdot Wind_{\max} \quad (9b)$$

where $\mu i$is the expected count (*CDI_count*) for station–month*i*, πi is the probability that station–month *i* belongs to the "SDS happen" state (*CDI_prob*); β_k and γ_k are regression coefficients for the *CDI_count* and *CDI_prob* components, respectively.

Model performance was evaluated using the coefficient of determination (R^2) and standard error metrics (RMSE and MAE). The standardised regression coefficients and their significance levels were used to quantify the relative contribution of each predictor to SDS occurrence and frequency. Because our primary objective is to infer process relationships rather than to develop an operational forecasting tool, the models were fitted to the full 2001–2024 station–month data set for each vegetation-cover group and evaluated using these goodness-of-fit diagnostics and residual cheques, rather than a separate training/validation split.

(4) Structural equation modelling (SEM)

To further disentangle the direct and indirect pathways by which climate and surface conditions influence dust activity, we used structural equation modelling (SEM). SEM is a confirmatory multivariate statistical framework, and is applied here to test a hypothesised eco-hydrological network linking drought, snow, soil moisture, vegetation, wind speed and dust activity, rather than to build an operational prediction model.

For the SEM analysis, the same 632 meteorological stations covering March–May for the period 2003–2023, which reflects the overlap between the dataset (Table 1), were applied. At each station, the response variable is the monthly dust index (*CDI*), and the explanatory variables are constructed at the same station locations and monthly resolution. Wind speed and drought conditions are derived from station-based meteorological records, while vegetation indices, snow metrics, soil moisture, and evapotranspiration components are obtained as spatial averages within a 30 km buffer around each station from the corresponding gridded products.

Separate SEMs were fitted for low- and high-vegetation regimes (FVC < 0.5 and FVC ≥ 0.5) to allow the pathways to differ with vegetation cover. The models include paths from snow cover and snowmelt timing to soil moisture, vegetation and drought (*SPEI*), from these variables to wind speed and evapotranspiration, and ultimately to *CDI*, thereby capturing both direct and indirect effects. SEMs were fitted in AMOS v. 21.0 using the covariance matrix of the observed variables. Model adequacy was assessed using standard fit indices: the Root Mean Square Error of Approximation (RMSEA), the Standardised Root Mean Square Residual (SRMR) and the Comparative Fit Index (CFI), with RMSEA < 0.05, SRMR < 0.08 and CFI > 0.90 taken to indicate an acceptable fit (Guo et al. 2022; Kakeh et al. 2023). The Tucker–Lewis Index (TLI) was also reported in the Supplementary Information.

3. Results

3.1. Trends in dust activity: evidence of northward movement

Between 2001 and 2024, regions with an annual average *DOD* greater than 0.2 were predominantly located in the desert and sandy areas of northern China and southern Mongolia, including the Taklamakan Desert,

Gurbantünggüt Desert, Kumtag Desert, Qaidam Basin Desert, Badain Jaran Desert, Tengger Desert, Ulan Buh Desert, Kubuqi Desert, Mu Us Desert, Hunshandake Desert, Khorchin Sandy Land, Great Gobi, Eastern Gobi Desert Steppe, and Gobi Lakes Valley desert steppe. In addition, areas downwind of deserts or at the desert edges, such as the Hexi Corridor and the western Loess Plateau, also exhibited higher *DOD* values. Among these regions, the Taklamakan Desert had the highest annual average *DOD*, the most days with *DOD* > 0.2, and the highest *CDI* values recorded at its meteorological stations (Figure 1 and Figure S2).

From an interannual perspective, the "desert edge area" showed a slight decreasing trend in spring *DOD* from 2001 to 2024 (-0.000014/year), with the frequency of dust events (number of days with *DOD* > 0.2) also decreasing at a rate of -0.00516/year. The *CDI* index peaked in 2016, then declined sharply from 2016 to 2019, with a slight recovery in recent years. Monthly trends indicated that April experienced the most significant decrease in dust activity, while March and May saw a slight resurgence in dust events (Figure 2 and Figure S3).

Spatially, dust activity exhibited a distinct "northward shift" pattern. In the southern desert edges (such as the Mu Us Desert, southern Qaidam Basin, southern Tengger Desert, and around the Taklamakan Desert), *DOD* and the frequency of days with *DOD* > 0.2 significantly decreased, with the most pronounced decline in the Mu Us Desert. In contrast, northern regions (including the northern Gurbantünggüt Desert, Badain Jaran Desert, southern Mongolian grasslands, northern Khorchin Sandy Land, Great Gobi, Eastern Gobi Desert Steppe, and Gobi Lakes Valley desert steppe) saw a significant increase in *DOD*. The *CDI* index changes aligned with this spatial trend, although some areas on the periphery of the Taklamakan Desert showed an increase in *CDI*, despite satellite observations not detecting significant increases in *DOD*. This discrepancy may stem from differences in observation methods—station-based measurements rely on wind speed and visibility, whereas satellites detect aerosol concentrations.

In summary, while overall spring dust activity in East Asia has not changed drastically since 2001, the spatial pattern has shifted, with a trend of dust activity moving northward.

3.2. Comparison of snow and vegetation's impact on dust activity

Comparative partial correlation analysis reveals that in areas with low vegetation cover, snow cover during the winter and spring seasons is significantly negatively correlated with SDS activity in the following year. The impact of snow cover on *DOD*, *DSF*, and *CDI* is notably stronger than that of the vegetation index during the same period, with these differences being statistically significant at $p = 0.05$. As vegetation cover increases, the difference in partial correlation coefficients between snow cover and dust activity gradually diminishes. Specifically, when fractional vegetation coverage (FVC) exceeds 0.5~0.7, the vegetation index has a stronger influence on *DOD* and *DSF* than winter and spring snow cover (SCF_{pre3}), highlighting that in high-vegetated areas, the importance of vegetation status increases. However, in low-vegetated areas, winter snow cover remains the dominant factor influencing the interannual variability of SDS in the subsequent year (Figure 3).

Since the partial correlation analysis only considered maximum wind speed, vegetation index, and snow cover during the winter and spring seasons, it may have overlooked the impact of other potential variables on SDS. To further clarify the driving mechanisms, this study employed a generalised linear model (i.e. ZINB) that incorporated a broader set of variables, including different vegetation indices, humidity indicators, snow parameters, and wind speed indicators. After filtering out highly co-linear variables using the variance inflation factor (VIF), the key variables shown in Figure 4 were selected. The results indicate that these variables explain 35% of the variation in SDS in low-vegetated (FVC < 0.5) areas and 31% in high-vegetated (FVC ≥ 0.5) areas.

Figure 4a shows the standardised regression coefficients for each variable when modelling the probability of SDS occurrence. In low-vegetated areas (FVC < 0.5), increased maximum and average wind speeds significantly raised the probability of SDS occurrence, while increased snow cover frequency during the previous three months (SCF_{pre3}) significantly reduced this probability. Additionally, the current month's vegetation index, snow cover, and moisture index ($SPEI_3$) also showed a negative impact, passing the significance test at $p = 0.05$, but their standardised coefficients were much smaller than those of wind speed and SCF_{pre3}. In areas with FVC ≥ 0.5, the impact of snow during the previous three months became

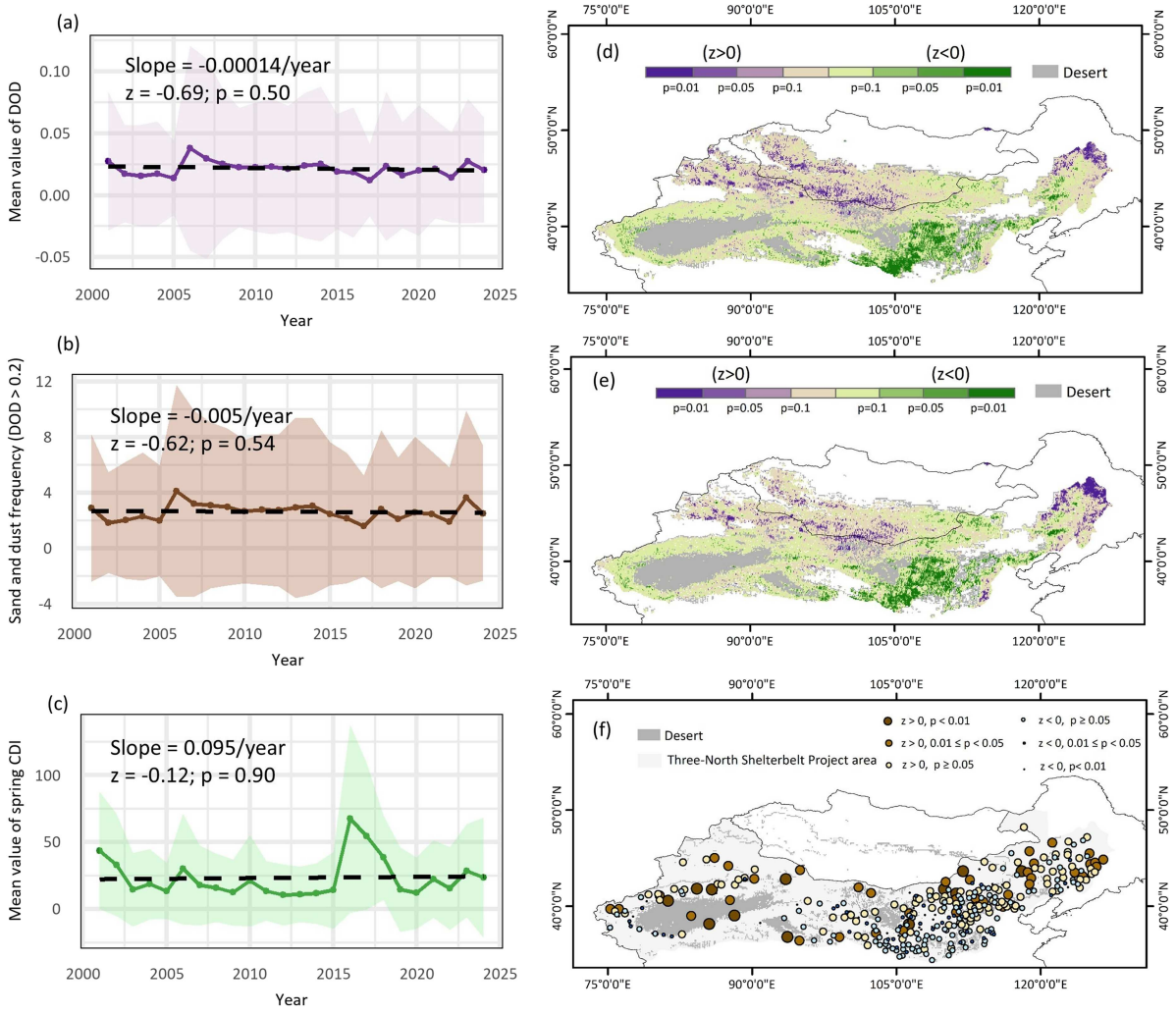

Figure 2. Spatiotemporal trends in spring dust activity at the desert margins of East Asia during 2001–2024. Panels (a), (b), and (c) show the interannual evolution of regional mean dust optical depth (*DOD*), dust storm frequency (*DSF*; days with *DOD* > 0.2), and the station-based comprehensive dust index (*CDI*) for March–May. Shaded areas indicate ± 1 standard deviation across grid cells (for *DOD* and *DSF*) or stations (for *CDI*). For each panel, the fitted linear trend (slope, per year) and the corresponding Mann–Kendall test statistic (z) and *p*-value for 2001–2024 are reported. Panels (d), (e), and (f) show the spatial distribution of MK z values for *DOD*, *DSF*, and *CDI*, respectively. Positive (negative) z values indicate increasing (decreasing) trends. The significance of trends is categorised into four levels based on the MK p-value: $p < 0.01$, $0.01 \le p < 0.05$, $0.05 \le p < 0.1$, and $p \ge 0.1$.

insignificant, with SDS occurrence primarily driven by maximum wind speed. Vegetation cover and snow increase during the current month helped to suppress SDS occurrence to a lesser extent.

Figure 4b shows the standardised coefficients for each variable when modelling the frequency of SDS occurrences. In low-vegetated areas, snow cover frequency during the previous three months (SCF_{pre3}) was the most critical factor affecting SDS frequency, with the strongest negative effect, indicating that more snow cover during winter and spring leads to a lower frequency of SDS. Meanwhile, increased wind speed, especially maximum wind speed, also raised SDS frequency, though its impact was slightly weaker than that of SCF_{pre3}. Vegetation-related variables, such as *NDVI*, $NDVI0.1_{ratio}$, and $NDVI0.3_{ratio}$, showed some uncertainty. This could be due to insufficient moisture in low-vegetated areas, making it difficult for vegetation to form effective coverage barriers.

In summary, in low-vegetated areas, SDS are mainly driven by enhanced wind speeds and reduced snow cover, with snow cover frequency during the previous three months being the most critical factor in

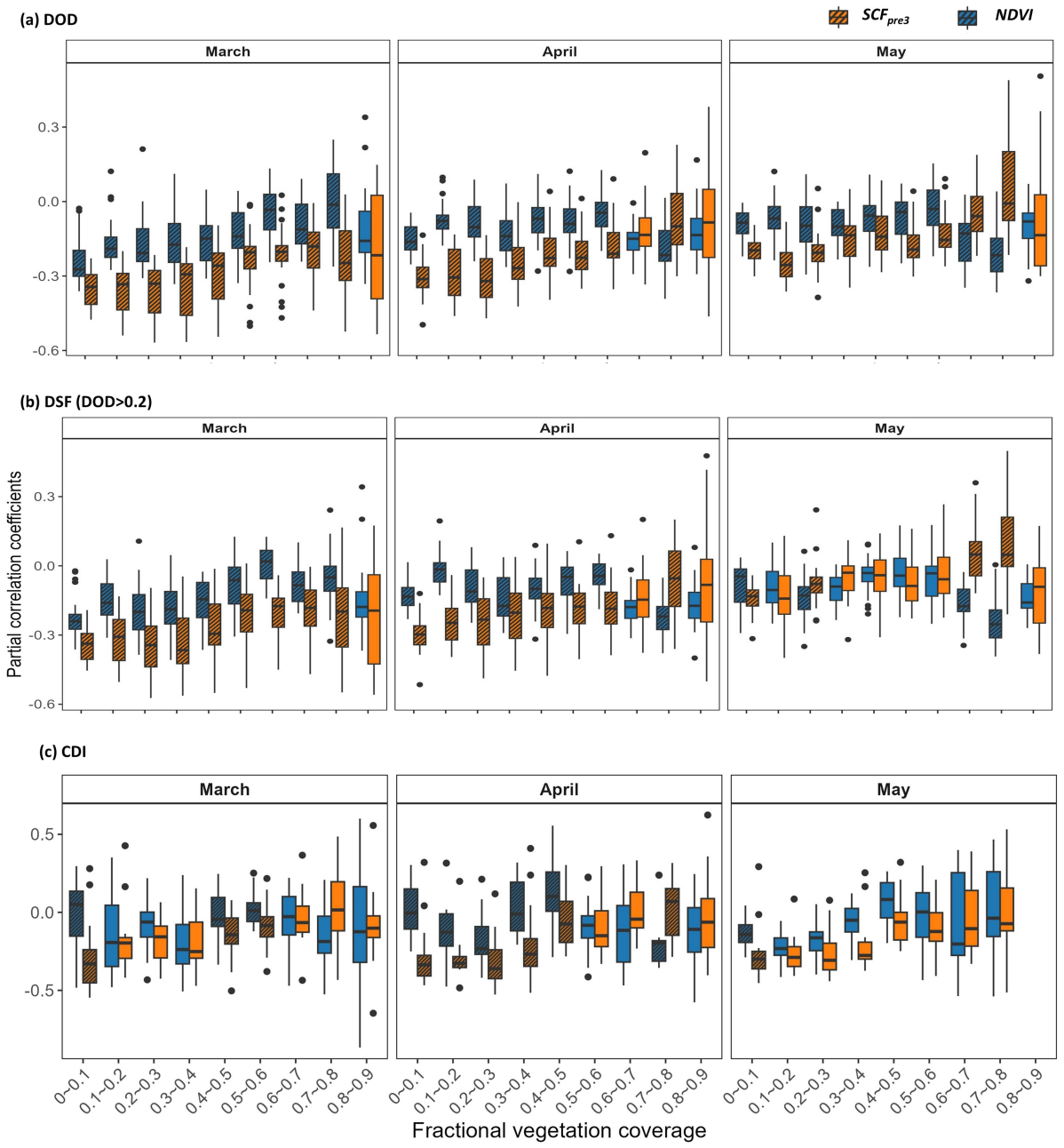

Figure 3. Partial correlation coefficients between dust activity and pre-season snow cover and vegetation index across different fractional vegetation coverage (FVC). The striped areas indicate significant differences in the correlation coefficients between pre-season snow cover and vegetation index ($p < 0.05$). Panel (a) represents dust activity as dust optical depth (*DOD*) from MODIS DB Collection 6.1 aerosol products; panel (b) represents dust activity frequency (*DSF*, the number of days when *DOD* > 0.2); and panel (c) represents dust activity as the comprehensive dust index (*CDI*), calculated based on observation records of floating dust, blowing sand, and SDS.

suppressing SDS, even more influential than wind speed. In high- vegetated areas, maximum wind speed is the dominant factor, while vegetation also contributes to reducing SDS occurrence.

3.3. Drivers of shifting dust activity under diverse vegetation coverage

To further elucidate the specific mechanisms by which vegetation and snow influence wind and sand activities under different vegetation cover conditions, this study uses SEM to explore the influence

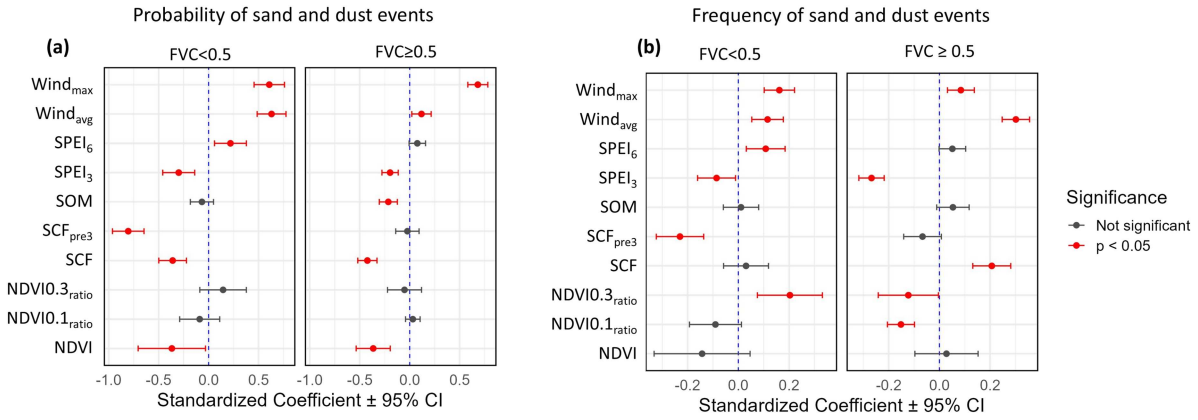

Figure 4. Standardised ZINB regression coefficients for modelling the probability of SDS occurrence (a) and dust frequency (b). Two separate plots are presented: the first plot focuses on the zero-inflation component, illustrating the effects of predictors on the probability of observing dust events; the second plot highlights the effect of predictors on the frequency of dust events (count component), showing the standardised coefficients and their 95% confidence intervals for each group. In both plots, significance is indicated by colouring the points red for significant predictors ($p < 0.05$) and grey for non-significant predictors.

pathways among factors such as vegetation, snow cover, wind speed, and evapotranspiration. The analysis was conducted under two scenarios: when fractional vegetation cover (FVC) is less than 0.5 and when it exceeds 0.5. To ensure temporal consistency, reduce data uncertainty, and minimise human interference, data from March to May each year were used. The model's goodness of fit is shown in Table S1.

There are significant differences in the formation pathways and eco-hydrological driving mechanisms of spring SDS under different vegetation cover areas (Figure 5). The results from the structural equation modelling show that wind speed is the most dominant factor driving SDS in both regions. In areas where FVC is less than 0.5, the positive path coefficient for wind speed on the comprehensive dust index (*CDI*) is 0.22 ($p < 0.05$), indicating that enhanced wind speed significantly exacerbates SDS. However, the vegetation's role in reducing wind speed is weak (path coefficient of -0.01), making it difficult to form an effective windbreak or sand-blocking function. At this stage, SDS is more influenced by the combined effects of climate and surface processes: winter snow increases soil moisture (path coefficient of 0.57, $p < 0.05$), and subsequent snowmelt recharges the upper soil layers, facilitating soil crusts formation, litter accumulation, and root development, thereby stabilising the substrate and reducing the supply of loose, fine particles available for deflation. Consequently, even when synoptic conditions are favourable for dust uplift, the frequency of SDS events tend to be lower than under drier conditions. (Figure 5a).

In contrast, in areas where FVC is greater than 0.5, the effect of wind speed on SDS is more significant (path coefficient of 0.31, $p < 0.05$). Meanwhile, vegetation becomes the key regulatory factor in controlling SDS by reducing wind speed (path coefficient of -0.27). Although the direct impact of snow cover, soil moisture index, and vegetation on *CDI* is relatively small (path coefficients all < 0.1), these variables play a service role in regulating the eco-hydrological environment of dust source areas by influencing wind speed and surface soil erodibility. In these areas, excessive snow cover may delay soil thawing and inhibit early spring vegetation greening, weakening evapotranspiration. Thus, winter snow cover is negatively correlated with spring vegetation index. Additionally, an increase in humidity typically corresponds to adequate moisture and vigorous plant transpiration, helping to enhance the ecosystem's buffering capacity against SDS (Figure 5b).

Overall, in low-vegetated areas, dust formation is more strongly influenced by moisture conditions shaped by winter snow, while wind speed remains a key factor but is less affected by vegetation. In high-vegetated areas, wind speed still plays a major role in dust occurrence; however, dense vegetation can substantially reduce wind speed, making it the most effective factor in suppressing SDS.

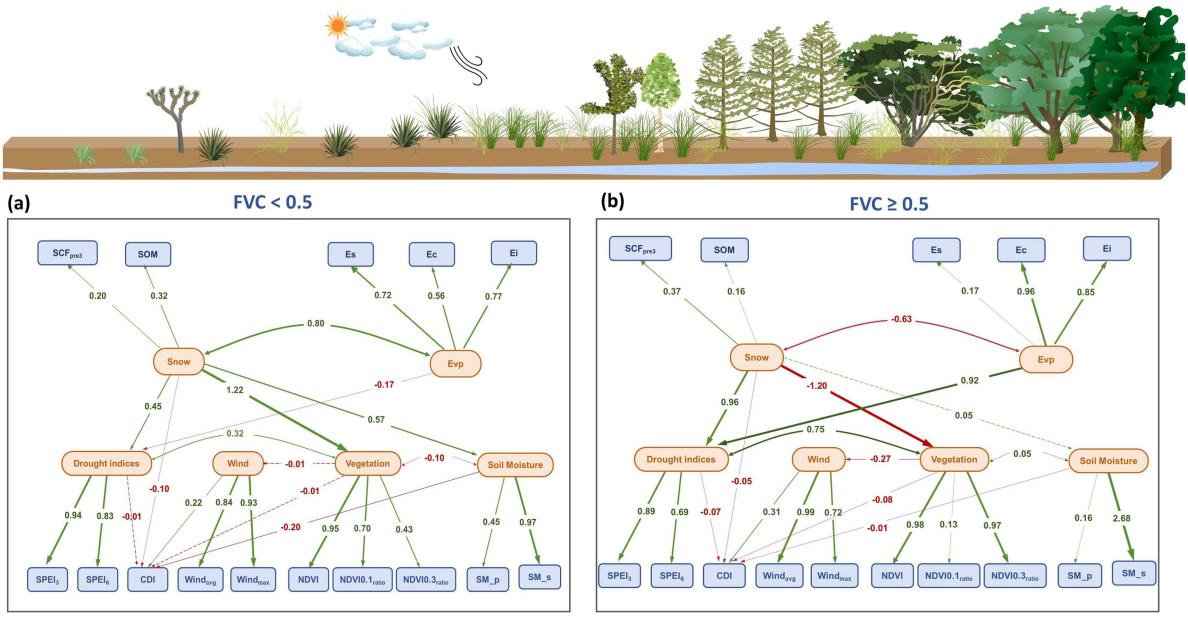

Figure 5. Structural equation modelling (SEM) results for the drivers and pathways of spring dust activity (*CDI*) at the desert margins of East Asia, based on March–May data from 2003 to 2023. The SEM assumes that dust activity is primarily controlled by wind, vegetation, humility, and snow-related variables. Latent variables are represented by orange ellipses and observed indicators by blue rectangles. Arrows denote hypothesised directional effects among latent and observed variables, and the numbers on the arrows are standardised path coefficients estimated by the SEM. Line thickness is proportional to the absolute value of the standardised coefficient. Green arrows indicate positive effects, red arrows indicate negative effects. Solid arrows denote statistically significant paths ($p < 0.05$), whereas dashed arrows represent non-significant paths that are retained to show the hypothesised causal structure. (a): SEM results for stations with fractional vegetation cover (FVC) < 0.5; (b): SEM results for FVC ≥ 0.5.

4. Discussion

4.1. Driving factors of dust activity change with vegetation cover: snow is the dominant factor in low-vegetated areas

This study found that the control exerted by snow exhibits marked spatial variability and dominates in regions where vegetation cover is low. Both the structural equation modelling and the generalised linear model indicate that, in these areas, the frequency of winter–spring snow cover (SCF_{pre3}) has a strongly negative effect on both the probability and frequency of dust-storm weather, with an intensity significantly greater than that of vegetation or moisture indices. Two mechanisms underlie this control: first, winter snow acts as a major water input, alleviating early-spring surface desiccation and reducing wind erosion of bare soil (Yang, Peng, and Dan 2025); second, snow cover delays the exposure of the soil surface, effectively narrowing the window during which spring winds can entrain sand and dust (Wu et al. 2022; Yang, Peng, and Dan 2025). By contrast, although wind speed remains the most direct driver in high-cover areas (FVC ≥ 0.5), vegetation exerts an indirect buffering effect by reducing wind speed, while snow's direct influence on dust weather is comparatively weak (Wu et al. 2022). This shift in control mechanisms demonstrates that, under low-vegetated conditions, snow rather than vegetation is the critical factor governing dust transport.

4.2. Northward migration of dust activity closely linked to diminishing snow: vegetation recovery alone is insufficient in combating dust activity

From 2001 to 2024, both MODIS *DOD* and station-based *CDI* data reveal a pronounced northward migration in the centre of dust activity: frequencies decreased markedly in southern source areas (e.g. Mu Us Desert,

southern Tengger Desert) but increased in southern Mongolia and northwestern China (e.g. northern Gurbantünggüt Desert, Great Gobi, Eastern Gobi Desert Steppe, and Gobi Lakes Valley desert steppe). This trend cannot be explained simply by a "lack of afforestation in Mongolia" or "insufficient vegetation recovery". Indeed, under global warming, springtime vegetation productivity in northern regions has generally risen (the "greening" trend in *NDVI*) with no large-scale degradation (Yu et al. 2003; Zhao et al. 2023). However, remote sensing shows that winter snow depth, frequency, and duration have declined across Mongolia and northern China (Figure S4). As a result, snow's dust-suppression effect is waning, exposing dry, bare soils in early spring as new desert dust sources. Therefore, on the low-cover desert margins, the retreat of snow is the core ecological driver of the northward shift in dust activity, rather than solely afforestation deficits or inadequate desert-control measures.

4.3. Implications

Our findings suggest that China's ambitious tree-planting initiatives along desert margins (e.g. Taklamakan, Badain Jaran, Tengger, Ulan Buh) are unlikely to deliver the expected reductions in dust-storm weather given current global warming trends. Previous studies have noted that edge-zone vegetation restoration often relies on intensive irrigation, depleting groundwater, and pitting agricultural, urban, and ecological water demands against one another—ultimately leading to transient vegetation recovery followed by decline (Wang et al. 2011; Han et al. 2020). This study adds a new perspective: vegetation mitigates dust primarily by weakening surface wind speeds, but in low-cover areas it functions as isolated barriers, unable to form a continuous, effective windbreak network. Only when vegetation coverage reaches a high level can a coherent wind corridor develop to attenuate wind speed and fix sand effectively. Achieving such high cover in natural source-edge environments requires rigorous maintenance, replanting, and irrigation; any drought, frost damage, or trampling instantly degrades coverage and protection. In contrast, winter snow, with its continuous, uniform cover and enhanced surface cohesion, suppresses wind erosion and dust much more effectively than sparse vegetation.

Thus, relying solely on large-scale afforestation or shrub-planting is both costly (financially and in terms of water) and yields limited wind and sand control benefits under low-cover conditions, making such projects prone to underperformance. Moreover, if efforts focus only on greening surfaces without measures to preserve snow cover or suppress desert dust sources, dust-storm hazards will remain unmitigated. We therefore recommend prioritising afforestation in desert-edge zones where natural precipitation is relatively ample, groundwater levels are higher, and wind erosion is most severe—avoiding blind planting in hyper-arid areas. In low-cover regions, project strategies should shift toward semi-natural reinforcement methods that combine engineering and ecological restoration. Concurrently, snow fences, artificial windbreaks, and surface mulches (e.g. biological mats, mineral films) should be deployed to retain snow cover during winter and spring, thereby reducing exposed sandy surfaces at the source.

The present study has provided an integrated, observation-based assessment of the drivers of spring SDS activity in East Asia, highlighting the key role of snow cover in sparsely vegetated regions. Building on these results, several extensions can be envisaged. First, a positive feedback is likely whereby desert dust deposited on seasonal snowpacks lowers surface albedo, accelerates snowmelt and lengthens the period during which bare, erodible surfaces are exposed (Gautam et al. 2013; Clow, Williams, and Schuster 2016); this dust–snow–SDS feedback was not explicitly quantified here, but could be examined by coupling the present surface-process framework with snow–albedo and surface energy-balance models. Secsond, large-scale atmospheric circulation could be incorporated more explicitly by linking the framework to indices describing the Mongolian cyclone and broader mid-latitude circulation regimes (Liu et al. 2020), thereby clarifying how circulation modulates snow, wind and SDS occurrence. Third, further progress is expected to benefit from improved ground-based observations in Mongolia: at present, station-based dust and meteorological analyses can be carried out only for northern China, whereas conditions in Mongolia are inferred from satellite and reanalysis products. The establishment of a coordinated, long-term Chinese–Mongolian SDS monitoring network with harmonised observing standards and event coding would greatly strengthen cross-border assessments of SDS dynamics and dust-source attribution in the East Asian desert margins.

5. Conclusion

This study shows that between 2001 and 2024, although the overall intensity of dust activity in East Asia exhibited only slight changes, its spatial pattern has undergone significant restructuring: the centre of dust activity has shifted northward, with a spatial trend of increasing intensity in the north and decreasing intensity in the south. While wind speed has remained a key driving factor for dust activity, the vegetation-ecology-hydrology processes enabling or constraining dust activity vary depending on surface cover: in low-vegetated areas, winter-spring snow plays a critical role in regulating soil moisture and spring vegetation, which is essential for suppressing dust frequency in the following year; in high-vegetated areas, maximum wind speed dominates, with vegetation gradually contributing to dust suppression.

In recent years, due to climate warming, winter-spring snow cover in northern China and southern Mongolia has decreased, leading to reduced spring moisture and exacerbating surface dryness. Under wind-driven conditions, active dust source areas have shifted northward toward drier sandy regions, likely intensifying in the future. Given that it requires intensive human investment and water resource use to maintain high vegetation cover in desert edge zones, large-scale afforestation projects in these areas often yield limited success and fail to effectively fix sand. Instead, precise measures are recommended in areas with relatively abundant natural precipitation, with priority given to semi-natural sand-fixation combinations (such as snow fences, artificial windbreaks, biological mats, or mineral films), thereby enhancing the sustainability and economic benefits of wind and sand control projects.

Author contributions

CRediT: Lilin Zheng — Conceptualisation, Methodology, Supervision, Writing – review & editing; Xia Lin — Data curation, Formal analysis, Visualisation; Annah Lake Zhu — Investigation, Resources; Ruishan Chen — Resources, Writing – review & editing; Ling Wang — review & editing.

Disclosure statement

We declare that we have no financial and personal relationships with other people or organisations that can inappropriately influence our work, there is no professional or other personal interest of any nature or kind in any product, service and/or company that could be construed as influencing the position presented in the manuscript entitled “Earlier Snowmelt is Driving the Northward Migration of East Asian Sand and Dust Storms”.

Funding

This work was supported by the Science and Technology Cooperation Programme of Shanghai Jiao Tong in Inner Mongolia Autonomous Region—Action Plan of Shanghai Jiao Tong University for "Revitalising Inner Mongolia through Science and Technology (Grant No. 25Z970300314), the Natural Science Foundation of Shanghai (Grant No. 24ZR1440400), the Young Talent Development Programme in the Humanities at Shanghai Jiao Tong University (2025QN034), and the Dutch Research Council (NWO) grant VI.Veni.201S.029.

ORCID

Lilin Zheng 0000-0002-6170-930X

Data availability statement

1) Meteorological dust observations (including floating dust, blowing sand, and SDS), along with other meteorological records (such as precipitation, temperature, wind speed, and evapotranspiration), were retrieved on 2025-05-01 from the China Meteorological Data Service Centre (https://data.cma.cn/en/?r=data/detail&dataCode=A.0012.0001), maintained by the China Meteorological Administration (2025). Grided meteorological data were obtained from https://cds.climate.copernicus.eu/datasets/reanalysis-era5-single-levels?tab=download, maintained by the Copernicus Climate Change Service (2017).
2) (MOD04_L2) platforms were retrieved on 2025-03-12 from https://ladsweb.modaps.eosdis.nasa.gov/archive/allData/61/MOD04_L2/, maintained by NASA's Earth Observing System Data and Information System (EOSDIS) (King et al., 1992).

Vegetation indices and fractional vegetation coverage were derived from MODIS reflectance products (MOD09A1 V6.1), accessed on 2025-03-12 from https://ladsweb.modaps.eosdis.nasa.gov/archive/allData/61/MOD09A1/, and maintained by the NASA EOSDIS Land Processes Distributed Active Archive (Vermote, 2021). Snow indices and phenology were provided by Hall and Riggs (2016), and were extracted from the MOD10A1 V6 Snow Cover Daily Global 500m product (https://nsidc.org/data/mod10a1/versions/61).

3) Evapotranspiration data, including vegetation transpiration (*Ec*), soil evaporation (*Es*), and interception from vegetation canopy (*Ei*) were provided by Zhang et al. (2019) and Gan et al. (2018); other supplementary data, such as the distribution of mobile and stabilised dunes were provided by Zheng et al. (2024).
4) Surface and profile soil moisture (SM_s and SM_p) were obtained from the GLDAS-2.2 Noah Land Surface Model products, accessed on 2025-12-01 from https://disc.gsfc.nasa.gov/datasets/GLDAS_NOAH025_M_2.2/summary, and maintained by the NASA Goddard Earth Sciences Data and Information Services Centre (Li et al. 2019).

Software

The statistical analysis in this study was conducted using R. Trend analysis was performed using the "terra" and "Kendall" packages; partial correlation analysis was carried out with the "ppcor" package; generalised linear models were constructed using the "glmmTMB" package; structural equation modelling was performed with the "lavaan" and "semTools" packages; and data visualisation of the above results was done using the "ggplot2" package.

References

Administration China Meteorological. 2025. *Basic Meteorological Observation Data on the Ground in China*. 457–477.

Amino, Tomomi, Yoshinori Iizuka, Sumito Matoba, Rigen Shimada, Naga Oshima, Toshitaka Suzuki, Takuto Ando, Teruo Aoki, and Kouji Fujita. 2021. "Increasing Dust Emission from Ice Free Terrain in Southeastern Greenland Since 2000." *Polar Science* 27: 100599. https://doi.org/10.1016/j.polar.2020.100599.

Anderson, Theodore L, Yonghua H Wu, D Allen Chu, Beat Schmid, Jens Redemann, and Oleg Dubovik. 2005. "Testing the MODIS Satellite Retrieval of Aerosol Fine-mode Fraction." *Journal of Geophysical Research-Atmospheres* 110 (D18): 20080002215. https://doi.org/10.1029/2005JD005978.

Bao, Tana, Guilin Xi, Baole Deng, IShin Chang, Jing Wu, and Erdemtu Jin. 2023. "Long-term Variations in Spatiotemporal Clustering Characteristics of Dust Events in Potential Dust Sources in East Asia." *Catena* 232: 107397. https://doi.org/10.1016/j.catena.2023.107397.

Chen, Siyu, Dan Zhao, Jianping Huang, Jiaqi He, Yu Chen, Junyan Chen, Hongru Bi, et al. 2023. "Mongolia Contributed More than 42% of the Dust Concentrations in Northern China in March and April 2023." *Advances in Atmospheric Sciences* 40 (9): 1549–1557. https://doi.org/10.1007/s00376-023-3062-1.

Cheng, Kai, Haitao Yang, Yuling Chen, Zekun Yang, Yu Ren, Yixuan Zhang, Danyang Lin, et al. 2025. "How Many Trees are there in China?" *Science Bulletin* 70(7): 1076–1079. https://doi.org/10.1016/j.scib.2025.02.001.

Clow, David W., Mark W. Williams, and Paul F. Schuster. 2016. "Increasing Aeolian Dust Deposition to Snowpacks in the Rocky Mountains Inferred from Snowpack, Wet Deposition, and Aerosol Chemistry." *Atmospheric Environment* 146: 183–194. https://doi.org/10.1016/j.atmosenv.2016.06.076.

D'Odorico, Paolo, Kelly Caylor, Gregory S. Okin, and Todd M. Scanlon. 2007. "On Soil Moisture-vegetation Feedbacks and their Possible Effects on the Dynamics of Dryland Ecosystems." *Journal of Geophysical Research-Biogeosciences* 112 (G4): G04010. https://doi.org/10.1029/2006JG000379.

Faroughi, Pouya, and Noriszura Ismail. 2017. "Bivariate Zero-inflated Negative Binomial Regression Model with Applications." *Journal of Statistical Computation and Simulation* 87(3): 457–477. https://doi.org/10.1080/00949655.2016.1213843.

Filonchyk, Mikalai. 2022. "Characteristics of the Severe March 2021 Gobi Desert Dust Storm and Its Impact on Air Pollution in China." *Chemosphere* 287: 132219. https://doi.org/10.1016/j.chemosphere.2021.132219.

Gan, Rong, Yongqiang Zhang, Hao Shi, Yuting Yang, Derek Eamus, Lei Cheng, Francis HS Chiew, and Q. Yu. 2018. "Use of Satellite Leaf Area Index Estimating Evapotranspiration and Gross Assimilation for Australian Ecosystems." *Ecohydrology* 11 (5): e1974. https://doi.org/10.1002/eco.1974.

Gao, Xin, Clement Narteau, and Cyril Gadal. 2021. "Migration of Reversing Dunes Against the Sand Flow Path as a Singular Expression of the Speed-Up Effect." *Journal of Geophysical Research-Earth Surface* 126(5. e2020JF005913. https://doi.org/10.1029/2020JF005913.

Gautam, Ritesh, N. Christina Hsu, William K. M. Lau, and Teppei J. Yasunari. 2013. "Satellite Observations of Desert Dust-induced Himalayan Snow Darkening." *Geophysical Research Letters* 40(5): 988–993. https://doi.org/10.1002/grl.50226.

Ginoux, Paul, Joseph M. Prospero, Thomas E. Gill, N. Christina Hsu, and Ming Zhao. 2012. "Global-Scale Attribution of Anthropogenic and Natural Dust Sources and Their Emission Rates Based on MODIS Deep Blue Aerosol Products." *Reviews of Geophysics* 50 (3): RG3005. https://doi.org/10.1029/2012RG000388.

Guo, Yujie, Zhibin Ren, Yulin Dong, Nanlin Hu, Chengcong Wang, Peng Zhang, Guangliang Jia, and Xingyuan He. 2022. "Strengthening of Surface Urban Heat Island Effect Driven Primarily by Urban Size Under Rapid Urbanization: National Evidence from China." *GIScience & Remote Sensing* 59(1): 2127–2143. https://doi.org/10.1080/15481603.2022.2147301.

Hall, D. K., V. V. Salomonson, and G. A. Riggs. 2021a. *MODIS/Terra Snow Cover Daily L3 Global 500m SIN Grid. (MOD10A1, Version 61)*. Boulder, Colorado USA: NASA National Snow and Ice Data Center Distributed Active Archive Center.

Hall, Dorothy K., George A. Riggs, Vincent V. Salomonson, Nicolo E. DiGirolamo, and Klaus J. Bayr. 2002. "MODIS Snow-cover Products." *Remote Sensing of Environment* 83(1): 181–194. https://doi.org/10.1016/S0034-4257(02)00095-0.

Hall, Dorothy K., Donal S. O'Leary, III, Nicolo E. DiGirolamo, Woodruff Miller, and Do Hyuk Kang. 2021b. "The Role of Declining Snow Cover in the Desiccation of the Great Salt Lake, Utah, Using MODIS Data." *Remote Sensing of Environment* 252: 112106. https://doi.org/10.1016/j.rse.2020.112106.

Hamed, Khaled H., and A. Ramachandra Rao. 1998. "A Modified Mann-kendall Trend Test for Autocorrelated Data." *Journal of Hydrology* 204(1): 182–196. https://doi.org/10.1016/S0022-1694(97)00125-X.

Han, Zhiming, Shengzhi Huang, Qiang Huang, Qingjun Bai, Guoyong Leng, Hao Wang, Jing Zhao, X. Wei, and X. Zheng. 2020. "Effects of Vegetation Restoration on Groundwater Drought in the Loess Plateau, China." *Journal of Hydrology* 591: 125566. https://doi.org/10.1016/j.jhydrol.2020.125566.

He, Lian, Haihan Hu, Fengming Hui, Xiao Cheng, Zhaojun Zheng, and Tao Che. 2024. "A New Snow Cover Mapping Algorithm for Chinese Geostationary Meteorological Satellite FY-4A AGRI Data." *International Journal of Digital Earth* 17 (1): 2367086. https://doi.org/10.1080/17538947.2024.2367086.

Jiang, Nan, Miaogen Shen, and Zhiyong Yang. 2025. "Advanced Vegetation Green-up Onset in Regions with Cooling Air Temperatures in the Northern Hemisphere: Drivers and Impacts on Productivity." *Global and Planetary Change* 252: 104891. https://doi.org/10.1016/j.gloplacha.2025.104891.

Kakeh, Jalil, Anvar Sanaei, Emma J. Sayer, Shadi Hazhir, Manouchehr Gorji, and Mohammad Hossein Mohammadi. 2023. "Biocrust Diversity Enhances Dryland Saline Soil Multifunctionality." *Land Degradation & Development* 34(2): 521–533. https://doi.org/10.1002/ldr.4476.

Kim, Dongchul, Mian Chin, Greg Schuster, Hongbin Yu, Toshihiko Takemura, Paolo Tuccella, Paul Ginoux, et al. 2024. "Where Dust Comes From: Global Assessment of Dust Source Attributions With AeroCom Models." *Journal of Geophysical Research-Atmospheres* 129 (16): e2024JD041377. https://doi.org/10.1029/2024JD041377.

Kok, Jasper F., David A. Ridley, Qing Zhou, Ron L. Miller, Chun Zhao, Colette L. Heald, Daniel S. Ward, Samuel Albani, and Karsten Haustein. 2017. "Smaller Desert Dust Cooling Effect Estimated from Analysis of Dust Size and Abundance." *Nature Geoscience* 10(4): 274–278. https://doi.org/10.1038/ngeo2912.

Lee, Eun Hee, and Byung Ju Sohn. 2011. "Recent Increasing Trend in Dust Frequency Over Mongolia and Inner Mongolia Regions and Its Association with Climate and Surface Condition Change." *Atmospheric Environment* 45 (27): 4611–4616. https://doi.org/10.1016/j.atmosenv.2011.05.065.

Li, Bailing, Matthew Rodell, Sujay Kumar, Hiroko Kato Beaudoing, Augusto Getirana, Benjamin F. Zaitchik, Luis Gustavo de Goncalves, et al. 2019. "Global GRACE Data Assimilation for Groundwater and Drought Monitoring: Advances and Challenges." *Water Resources Research* 55(9): 7564–7586. https://doi.org/10.1029/2018WR024618.

Li, Jiandong, Xin Hao, Hong Liao, Xu Yue, Hua Li, Xin Long, and Nan Li. 2022. "Predominant Type of Dust Storms That Influences Air Quality Over Northern China and Future Projections." *Earths Future* 10 (6): e2022EF002649. https://doi.org/10.1029/2022EF002649.

Lian, Xu, Sujong Jeong, Chang-Eui Park, Hao Xu, Laurent Z. X. Li, Tao Wang, Pierre Gentine, Josep Peñuelas, and Shilong Piao. 2022. "Biophysical Impacts of Northern Vegetation Changes on Seasonal Warming Patterns." *Nature Communications* 13(1): 3925. https://doi.org/10.1038/s41467-022-31671-z.

Liu, Jun, Dongyou Wu, Guangjing Liu, Rui Mao, Siyu Chen, Mingxia Ji, Pingqing Fu, et al. 2020. "Impact of Arctic Amplification on Declining Spring Dust Events in East Asia." *Climate Dynamics* 54(3): 1913–1935. https://doi.org/10.1007/s00382-019-05094-4.

Maki, Takashi, Taichu Y Tanaka, Tsuyoshi Koshiro, Atsushi Shimizu, Tsuyoshi T. Sekiyama, Mizuo Kajino, Yasunori Kurosaki, Toshiya Okuro, and Naga Oshima. 2022. "Changes in Dust Emissions in the Gobi Desert due to Global Warming Using MRI-ESM2.0." *SOLA* 18: 218–224. https://doi.org/10.2151/sola.2022-035.

Meinander, Outi, Pavla Dagsson-Waldhauserova, Pavel Amosov, Elena Aseyeva, Cliff Atkins, Alexander Baklanov, Clarissa Baldo, et al. 2022. "Newly Identified Climatically and Environmentally Significant High-latitude Dust Sources." *Atmospheric Chemistry and Physics* 22 (17): 11889–11930. https://doi.org/10.5194/acp-22-11889-2022.

Meinander, Outi, Andreas Uppstu, Pavla Dagsson-Waldhauserova, Christine Groot Zwaaftink, Christian Juncher Jørgensen, Alexander Baklanov, Adam Kristensson, Andreas Massling, and Mikhail Sofiev. 2025. "Dust in the Arctic: A Brief Review of Feedbacks and Interactions Between Climate Change, Aeolian Dust and Ecosystems." *Frontiers in Environmental Science* 13: 1536395. https://doi.org/10.3389/fenvs.2025.1536395.

Middleton, Nick J. 1991. "Dust Storms in the Mongolian People's Republic." *Journal of Arid Environments* 20(3): 287–297. https://doi.org/10.1016/S0140-1963(18)30690-6.

Naeimi, Maryam, Jian Chu, Mohammad Khosroshahi, and Leila Kashi Zenouzi. 2023. "Soil Stabilization for Dunes Fixation Using Microbially Induced Calcium Carbonate Precipitation." *Geoderma* 429: 116183. https://doi.org/10.1016/j.geoderma.2022.116183.

Natsagdorj, Luvsan, Dulam Jugder, and Y. S. Chung. 2003. "Analysis of Dust Storms Observed in Mongolia During 1937–1999." *Atmospheric Environment* 37(9): 1401–1411. https://doi.org/10.1016/S1352-2310(02)01023-3.

Park, Sunyurp, and Jinmu Choi. 2016. "Satellite-measured Atmospheric Aerosol Content in Korea: Anthropogenic Signals from Decadal Records." *GIScience & Remote Sensing* 53(5): 634–650. https://doi.org/10.1080/15481603.2016.1214351.

Piao, Shilong, Jianguang Tan, Anping Chen, Yongshuo H Fu, Philippe Ciais, Qiang Liu, Ivan A Janssens, et al. 2015. "Leaf Onset in the Northern Hemisphere Triggered by Daytime Temperature." *Nature Communications* 6: 6911. https://doi.org/10.1038/ncomms7911.

Pu, Bing, and Paul Ginoux. 2018. "How Reliable are CMIP5 Models in Simulating Dust Optical Depth?" *Atmospheric Chemistry and Physics* 18(16): 12491–12510. https://doi.org/10.5194/acp-18-12491-2018.

Savitzky, Abraham, and Marcel J E. Golay. 1964. "Smoothing and Differentiation of Data by Simplified Least Squares Procedures." *Analytical Chemistry* 36(8): 1627–1639. https://doi.org/10.1021/ac60214a047.

Service Copernicus Climate Change. 2017. ERA5: Fifth generation of ECMWF atmospheric reanalyses of the global climate. Copernicus Climate Change Service (C3S) Climate Data Store (CDS).

Smith, William K., Matthew P. Dannenberg, Dong Yan, Stefanie Herrmann, Mallory L. Barnes, Greg A. Barron-Gafford, Joel A. Biederman, et al. 2019. "Remote Sensing of Dryland Ecosystem Structure and Function: Progress, Challenges, and Opportunities." *Remote Sensing of Environment* 233: 111401. https://doi.org/10.1016/j.rse.2019.111401.

Tucker, Compton J. 1979. "Red and Photographic Infrared Linear Combinations for Monitoring Vegetation." *Remote Sensing of Environment* 8(2): 127–150. https://doi.org/10.1016/0034-4257(79)90013-0.

Vicente-Serrano, Sergio M., Santiago Beguería, and Juan I. López-Moreno. 2010. "A Multiscalar Drought Index Sensitive to Global Warming: The Standardized Precipitation Evapotranspiration Index." *Journal of Climate* 23(7): 1696–1718. https://doi.org/10.1175/2009JCLI2909.1.

Wang, Yunqiang, Mingan Shao, Yuanjun Zhu, and Zhipeng Liu. 2011. "Impacts of Land Use and Plant Characteristics on Dried Soil Layers in Different Climatic Regions on the Loess Plateau of China." *Agricultural and Forest Meteorology* 151(4): 437–448. https://doi.org/10.1016/j.agrformet.2010.11.016.

Wang, Shushan, Yan Yu, Xiaoxiao Zhang, Huayu Lu, Xiaoye Zhang, and Zhiwei Xu. 2021. "Weakened Dust Activity Over China and Mongolia from 2001 to 2020 Associated with Climate Change and Land-use Management." *Environmental Research Letters* 16 (12): 124056. https://doi.org/10.1088/1748-9326/ac3b79.

Wang, Li, Yanning Qiu, Zhiyong Han, Chi Xu, Shuang-Ye Wu, Yao Wang, and Milena Holmgren, et al. 2022. "Climate, Topography and Anthropogenic Effects on Desert Greening: A 40-year Satellite Monitoring in the Tengger Desert, Northern China." *Catena* 209: 10581.

Wu, Xiaoling, Chenglai Wu, Zhaohui Lin, and Mingzhu Yang. 2025. "Intra-seasonal Variations of Dust Activity Over East Asia in Spring 2023 and Their Mechanisms." *Global and Planetary Change* 244: 104638. https://doi.org/10.1016/j.gloplacha.2024.104638.

Wu, Chenglai, Zhaohui Lin, Yaping Shao, Xiaohong Liu, and Ying Li. 2022. "Drivers of Recent Decline in Dust Activity Over East Asia." *Nature Communications* 13(1): 7105. https://doi.org/10.1038/s41467-022-34823-3.

Yan, Yu, Zhiyong Liu, Lei Chen, Xiaohong Chen, Kairong Lin, Zhenzhong Zeng, Xin Lan, et al. 2025. "Earth Greening and Climate Change Reshaping the Patterns of Terrestrial Water Sinks and Sources." *Proceedings of the National Academy of Sciences of the United States of America* 122 (11): e2410881122. https://doi.org/10.1073/pnas.2410881122.

Yang, Lu, Shushi Peng, and Zhu Dan. 2025. "Extended Gap Between Snowmelt and Greenup Increases Dust Storm Occurrence." *Global Change Biology* 31 (5): e70236. https://doi.org/10.1111/gcb.70236.

Yao, Wenrui, Ke Gui, Hengheng Zhao, Linchang An, Nanxuan Shang, Xutao Zhang, Lei Li, et al. 2024. "Reconstruction of Historical Site-scale Dust Optical Depth (DOD) Time Series from Surface Dust Records and Satellite Retrievals in Northern China: Application to the Evaluation of DOD in CMIP6 Historical Simulations." *Journal of Climate* 37(23): 6253–6267. https://doi.org/10.1175/JCLI-D-23-0624.1.

Yin, Zhicong, Yu Wan, Yijia Zhang, and Huijun Wang. 2022. "Why Super Sandstorm 2021 in North China?" *National Science Review* 9 (3): nwab165. https://doi.org/10.1093/nsr/nwab165.

Yu, Fangfang, Kevin P Price, James Ellis, and PeiJjun Shi. 2003. "Response of Seasonal Vegetation Development to Climatic Variations in Eastern Central Asia." *Remote Sensing of Environment* 87 (1): 42–54. https://doi.org/10.1016/S0034-4257(03)00144-5.

Zhang, Xiao Y., Richard Arimoto, and Zhi S. An. 1997. "Dust Emission from Chinese Desert Sources Linked to Variations in Atmospheric Circulation." *Journal of Geophysical Research-Atmospheres* 102(D23): 28041–28047. https://doi.org/10.1029/97JD02300.

Zhang, Hongbo, Fan Zhang, Guoqing Zhang, Tao Che, Wei Yan, Ming Ye, and Ning Ma. 2019a. "Ground-based Evaluation of MODIS Snow Cover Product V6 Across China: Implications for the Selection of NDSI Threshold." *Science of the Total Environment* 651: 2712–2726. https://doi.org/10.1016/j.scitotenv.2018.10.128.

Zhang, Yongqiang, Dongdong Kong, Rong Gan, Francis HS Chiew, Tim R McVicar, Qiang Zhang, and Yuting Yang. 2019b. "Coupled Estimation of 500 m and 8-day Resolution Global Evapotranspiration and Gross Primary Production in 2002-2017." *Remote Sensing of Environment* 222: 165–182. https://doi.org/10.1016/j.rse.2018.12.031.

Zhao, Xiaohan, Fangmin Zhang, Qian Liu, Yunpeng Li, Yuanshu Jing, and Yanyu Lu. 2023. "Climate Change Overshadows Human Activities in Enhancing Vegetation Activity in Inner Mongolia." *Theoretical and Applied Climatology* 154(1-2): 245–259. https://doi.org/10.1007/s00704-023-04553-7.

Zheng, Zhijia, Jinsongdi Yu, Xiuyuan Zhang, and Shihong Du. 2024. "Development of a 30 m Resolution Global Sand Dune/sheet Classification Map (GSDS30) Using Multi-source Remote Sensing Data." *Remote Sensing of Environment* 302: 113973. https://doi.org/10.1016/j.rse.2023.113973.